Case Report

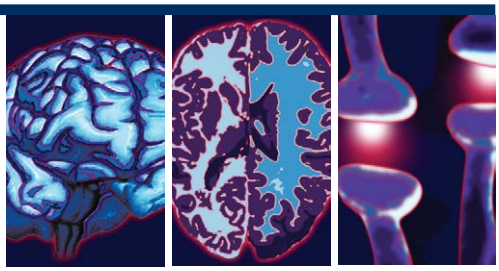

Maladaptive Reorganization in Pain-Related Brain Network Contributing To the Central Post-Stroke Pain

Xiaoyun Li[1], Yi Feng[2,†], Fei Gao[2,†]

ABSTRACT

Background

The underlying pathophysiological mechanisms of central post-stroke pain (CPSP) have not been well understood.

Case report

We collected data from a male CPSP patient with ischemic stroke lesions in the left secondary somatosensory cortex and left posterior insula for the investigation of behavioral-anatomical-functional alterations in CPSP, using somatosensory testing, diffusion tensor imaging (DTI), and resting-state functional magnetic resonance imaging (fMRI) techniques. Behavioral results showed that the patient was unable to detect non-nociceptive somatosensory stimuli delivered to the affected hand. Neuroimaging results displayed that compared to healthy controls, the CPSP patient showed (1) the disrupted microstructure (eg, axonal demyelination) in the spino-thalamo-cortical pathway, (2) the hyperactivity in the pain-related brain region (eg, anterior cingulate cortex, ACC) associated with central sensitization, and (3) the dysfunction of pain inhibitory pathways (eg, decreased functional connectivity between ACC and the right dorsolateral prefrontal cortex).

Conclusion:

These findings revealed a unique pattern of widespread structural and functional plasticity in the CPSP patient accompanied with somatosensory abnormalities, supporting the maladaptive reorganization model of pain networks in CPSP.

Keywords:

Central post-stroke pain (CPSP), Somatosensory testing, Diffusion tensor imaging (DTI), Functional magnetic resonance imaging (fMRI), Maladaptive reorganization

Abbreviations

ACC: Anterior cingulate cortex; AD: Axial diffsivity; AI: Anterior insula; BA: Brodmann area; CPSP: Central post-stroke pain; DLPFC: Dosolateral prefrontal cortex; DTI: Diffusion tensor imaging; fMRI: Functional magnetic resonance imaging; FA: Fractional anisotropy; FOV: Field of view; FWE: Family-wise error; KCC: Kendall's coefficient of concordance; MD: Mean diffusivity; MI: Primary motor cortex; NRS: Numerical rating scale; PI: Posterior

[1]Faculty of Psychology, Southwest University, Chongqing, China

[2]Department of Pain Medicine, Peking University People's Hospital, Beijing, China

[†]Author for correspondence: Fei Gao, Department of Pain Medicine, Peking University People's Hospital, Beijing, China, Tel: +86 13911628415; Fax: +86-10-88365950; email: gaofei19780318@sina.com

Yi Feng, Department of Pain Medicine, Peking University People's Hospital, Beijing, China, Tel: +86 13601083503; Fax: +86-10-88365950; email: yifeng65@sina.com

insula; RD: Radial diffusivity; ReHo: Regional homogeneity; ROIs: Regions of interest; rsfMRI: Resting-state functional magnetic resonance imaging; SI: Primary somatosensory cortex; SII: Secondary somatosensory cortex; TBSS: Tract-based spatial statistics; TE: Repetition time; TFCE: Threshold-Free Cluster Enhancement; THA: Thalamus; TR: Echo time

Introduction

Central post-stroke pain (CPSP), a central neuropathic pain, is one of the most troublesome sequelae of ischemic or hemorrhagic stroke. Epidemiological data show that about 1%-12% stroke accidents, occurred either at the thalamic level or at the non-thalamic level (eg, brainstem, medulla, and operculo-insula), may develop into the CPSP [1]. Majority patients with CPSP suffer continuous or intermittent, intractable pain spontaneously, contralateral to the brain lesions. Somatosensory abnormalities have been frequently reported in the CPSP patients, including dysesthesia, allodynia, and/or hyperalgesia [1,2]. As a refractory disease, about 50%-60% patients with CPSP are resistant to pharmacological (eg, anticonvulsant or antidepressant drugs) and non-pharmacological (eg, deep brain stimulation or motor cortex stimulation) treatments [1-3]. Therefore, CPSP may lead to a poor quality of life, pain-related sleep interference, and disruption of rehabilitation.

Unfortunately, the knowledge of pathophysiological mechanisms leading to CPSP is scarce, even though different theories have been proposed, including central sensitization and central disinhibition [1,4]. In particular, hyperexcitability of central neurons in pain-related regions, such as the thalamus, is contributed to the cause of spontaneous pain in some CPSP cases [5,6]. The disinhibition theory suggests that the development of spontaneous pain in the CPSP patients results from a loss of normal inhibitory inputs [1,6-8]. Recently, Hosomi et al. [2] have proposed that CPSP is considered as a maladaptive reorganization of pain network rather than a simple, progressive process of a focal lesion or pathway after stroke. Here we reported a CPSP case and employed a combination of somatosensory testing, diffusion tensor imaging (DTI), and resting-state functional magnetic resonance imaging (rsfMRI) techniques to investigate the behavioral-anatomical-functional alternations of CPSP to understand the underlying pathophysiological mechanisms, which would help develop the mechanism-based analgesic strategies in the future.

Material and methods

Case report

A 59-year-old right-handed male suffered a left hemispheric stroke causing right hemiplegia, abnormal temperature sensation, and tactile anesthesia on the right upper limb in winter 2014. Structural brain imaging revealed the ischemic stroke lesions in the left secondary somatosensory cortex (SII) and left posterior insula (PI; **Figure 1**). Six months after stroke, the patient experienced an intermittent dull pain on the right chest and right back with self-reported pain intensity of 4 on a 0–10 numerical rating scale (NRS), although he had improvements on the tactile and motor functions. Twelve months after stroke, the pain became severe with self-reported pain intensity of 7-8 on the NRS and expanded to right lower limb. Meanwhile, allodynia occurred on the right hand and right face. In August 2016, the pain extended to right upper limb and right head with self-reported pain intensity of 8-9 on the NRS. During the following four months, the patient received both pharmacological (ie, gabapentin and tramadol) and non-pharmacological (ie, transcranial magnetic stimulation) treatments. After the treatments, he had a transitory improvement of pain (about 10% reduction). In December 2016, the patient gave his written informed consent to participate the present study, and the local Ethics Committee approved the experimental procedures.

Twenty right-handed subjects were invited to participate the DTI-fMRI scanning secession as healthy controls (eight males; mean age ± standard deviation: 61.3±8.0 years). All control subjects had no history of chronic pain or psychiatric disorders. An expert radiologist confirmed that there was no cerebral damage or lesion in any of the healthy subjects. All subjects gave their written informed consent before the experiment.

Somatosensory testing

Prior to the MRI data collection, detection of painful and non-painful somatosensory sensations at both left and right sides of the CPSP patient were measured by using laser and electrical stimulation. The painful laser stimuli were generated by an infrared neodymium yttrium aluminium perovskite

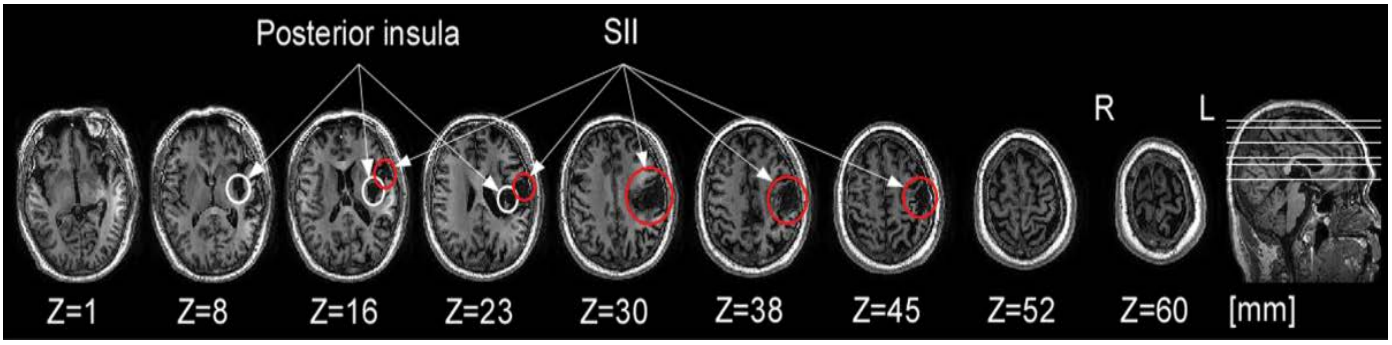

Figure 1: MRI scan of the patient. Axial sections of the T1-weighted image reveal severe brain lesions in the left posterior insula (indicated by white circles) and the left secondary somatosensory cortex (SII, indicated by red circles). The axial slices depicted correspond to Z=1, 8, 16, 23, 30, 38, 45, 52, and 60 in the MNI (Montreal Neurological Institute) space. L: left, R: right.

(Nd:YAP) laser (Electronical Engineering, Italy), delivered to the dorsum of either left or right hand. The parameters of laser stimuli were as following: wavelength=1.34 μm, laser beam diameter=7 mm, pulse duration=4 ms, stimulus intensity=3.5 J. The non-painful electrical stimuli were constant-current square-wave pluses (DS&A, Digitimer Ltd., UK) delivered to either left or right index finger, through a pair of ring electrodes (1 cm distance between electrodes). The parameters of electrical stimuli were as following: duration=0.5 ms, stimulus intensity=5 mA. In each body side, we delivered 30 painful stimuli and 30 non-painful stimuli in a pseudorandom order, with ~15 s per trial. During the evaluation period in each trial, the patient was required to report the perceived intensity of the stimulus verbally on the 0-10 NRS (0=no sensation, 10=extremely strong sensation). Paired-sample t-tests were performed to assess differences of the painful and non-painful somatosensory sensations between the affected and unaffected sides of the patient, respectively, using SPSS 16.0 statistical analysis package.

■ Imaging acquisition

MRI scanning was performed with a 3-Tesla GE whole body scanner (GE Healthcare, Waukesha, WI, USA) with an 8-channel head coil. A high-resolution three-dimensional structural T1-weighted image using a sagittal spoiled gradient echo sequence was acquired for each subject. The T1 parameters were as following: 176 sagittal slices, repletion time (TR)=6.9 ms, echo time (TE)=3 ms, flip angle= 8°, field of view (FOV)=256 mm, matrix=256×256, in-plane resolution=1×1×1 mm^3, total acquisition time=4.36 min. The rsfMRI scan was acquired using a gradient-echo planar sequence. Subjects were instructed to keep their eyes open, look at a white cross presented on the screen, without thinking about anything in particular. The rsfMRI parameters were as following: 37 axial slices, TR=2000 ms, TE=30 ms, flip angle=90°, FOV=220 mm, matrix=64×64, in-plane resolution=3.5×3.5×3.5 mm^3, spacing=0.5 mm, total acquisition time=10 min. The DTI scan was obtained using a single-shot spin-echo planar sequence. The DTI parameters were as following: 70 axial slices, TR=8500 ms, TE=80.8 ms, flip angle=90°, FOV=256 mm, matrix=128×128, in-plane resolution=2×2×2 mm^3, b=1000 s/mm^2, diffusion direction=64 directions, b0 images=1 image, total acquisition time=9.21 min.

■ Diffusion tensor imaging preprocessing and analysis

All DTI images were processed and analyzed with the tools in FSL software package (FMEIB Software Library, Oxford, UK, http://www.fmrib.ox.ac.uk/fsl). Initially, eddy current and head motion artifact correction was performed using FMRIN diffusion toolbox (FDT). Then, brain tissues were extracted using brain extraction tool (BET). A diffusion tensor model was applied to each voxel in the brain in order to generate a voxel-wise map of fractional anisotropy (FA) values for each individual subject using FDT. After that, tract-based spatial statistics (TBSS) analyses were performed. Individual FA maps were nonlinearly registered to the 1×1×1 mm^3 FMRIB58_FA standard-space template. All registered FA maps were averaged to generate and thin a mean FA template, in order to create a white matter skeleton representing

the white matter tracts that are most common across all subjects. This mean FA template was then thresholded to include only voxels with FA values of greater than 0.2, so as to only incorporate voxels indicative of white matter. Finally, individual aligned FA map was projected onto the mean FA skeleton.

The permutation-based non-parametric inferences were employed to detect the between-group differences (by using prediction interval test) in our study (with 5000 random permutations), after adjusting age and gender (https://fsl.fmrib.ox.ac.uk/fsl/fslwiki/GLM). Please note that we evaluated the possible gender differences of DTI images and rsfMRI images for healthy controls after controlling for age, and we observed no significant difference for both data. To increase the statistical power of our study, all 20 healthy control subjects were included in the analysis. The output contained statistical FA maps after correcting for multiple comparisons using Threshold-Free Cluster Enhancement (TFCE) with a family-wise error (FWE) correction (cluster threshold $p<0.05$). Other DTI properties, such as, mean diffusivity (MD), axial diffusivity (AD), and radial diffusivity (RD) were processed and analyzed in the same way.

In order to determine white matter abnormalities in pain-related regions, 12 brain regions were chosen as the regions of interest (ROIs), including bilateral ACC, anterior insula (AI), PI, primary somatosensory cortex (SI), SII, and thalamus (THA) [9]. The ACC and the THA were selected from the Harvard-Oxford Cortical and Subcortical Atlas (Harvard Center for Morphometric Analysis), thresholded at 25%. SI and SII were selected from Juelich Histological Atlas (The Research Center Juelich), thresholded at 25%. AI and PI were regions as defined by Cauda et al. [10]. All ROIs were transformed to the standard space, in consistent with the FMRIB58_FA template. For each subject, the mean values of FA, MD, AD, and RD in each of these 12 ROIs were extracted after mapping the masks in the standard template through the transformation.

Finally, prediction interval tests were performed to compare each DTI property (ie, FA, MD, AD, RD) at 12 ROIs of the CPSP patient with that of the average of healthy control subjects, respectively, using SPSS v16.0. Results for each diffusivity measure were corrected for multiple comparisons using Bonferroni correction for 12 comparisons ($p<0.0042$).

■ Resting state fMRI preprocessing and analysis

All rsfMRI images were processed and analyzed with the DPARSFA software (Data Processing Assistant for Resting-State fMRI, Advanced, http://www.restfmri.net), which is based on statistical parametric mapping (SPM; Welcome Trust Centre for Neuroimaging, University College London, United Kingdom, http://www.fil.ion.ucl.ac.uk/spm/). The first 10 time points of each rsfMRI image were removed, and the remaining 290 time points were corrected for slice timing and head motion. All subjects with head motion more than maximal translation of 1.5 mm and maximal rotation of 1.5° were excluded. The individual T1 image was coregistered to the functional image and then segmented into gray matter, white matter and cerebrospinal fluid. The functional images and the segmented T1 images were spatial normalized to standard MNI space template (with voxel size of 3 mm). Finally, the aligned functional images were linearly detrended, band-pass filtered at 0.01-0.08 Hz, and regressed the nuisance signal, including Friston 24 head motion parameters and signals from cerebrospinal fluid and white matter.

To investigate the regional brain activity during rest, regional homogeneity (ReHo) analysis was employed. Individual ReHo map was generated by calculating the Kendall's coefficient of concordance (KCC) of time series of a given voxel with those of its nearest neighborhood voxels (26 voxels) in a voxel-wise approach. Then, the ReHo data was spatially smoothed with a Gaussian kernel of FWHM 6 mm. Prediction interval test was performed to assess differences in the ReHo maps between the CPSP patient and healthy control subjects, using the second-level analysis in SPM8, after adjusting age and gender.

To further explore the abnormal intrinsic functional circuits in the CPSP patient, the peak voxel of brain regions showing significant group differences in ReHo was selected to create a 6 mm-radius sphere seed for seed-based functional connectivity analysis. Individual voxel-wise map, reflecting the correlation coefficient between the time course of the seed region and the time course of the remaining brain voxels was generated. Correlation coefficients were then transformed to z values using Fisher's r-to-z transformation to improve the normality of the distribution. Prediction interval test was performed to

assess differences in the seed-based functional connectivity maps between the CPSP patient and healthy control subjects, controlling for age and gender. The significant threshold was set at $p<0.05$ with a minimum cluster size of 202 voxels (5454 mm^3) and 10000 simulations, which corresponded to a corrected $p<0.05$ [11]. The correction was determined by Monte Carlo simulations, which were performed by the AlphaSim program in an rsfMRI data analysis toolkit (REST, 2.0; http://www.restfmri.net).

Results

Somatosensory testing

The difference of the perceived intensity of painful laser stimuli between affected (right) and unaffected (left) hands of the CPSP patient was not significant ($t(29)=0.5$, $p>0.05$). In contrast, the perceived intensity ratings of non-painful electrical stimuli delivered to the unaffected hand were significantly larger than those to the affected hand ($t(29)=12.9$, $p<0.001$; Figure 2).

TBSS analysis

The whole-brain voxel-wise TBSS analysis revealed that the patient showed a significant reduction in FA value and significant increases in MD and RD values ($p<0.05$, FWE-corrected; Figure 3), and these significant changes were mainly overlapped in the left postcentral gyrus, left superior longitudinal fasciculus, left posterior corona radiata, left posterior thalamic radiation, and left retrolenticular part of internal capsule (Table 1). These results implied that axons may be lacked of directional coherence (lower FA and higher MD) and be demyelinated (higher RD) in the regions of left SII and left PI, suggesting axonal demyelination in these regions for the CPSP patient due to ischemic stroke lesions.

ROI-based analyses revealed significant altered diffusion metrics of certain pain-related regions

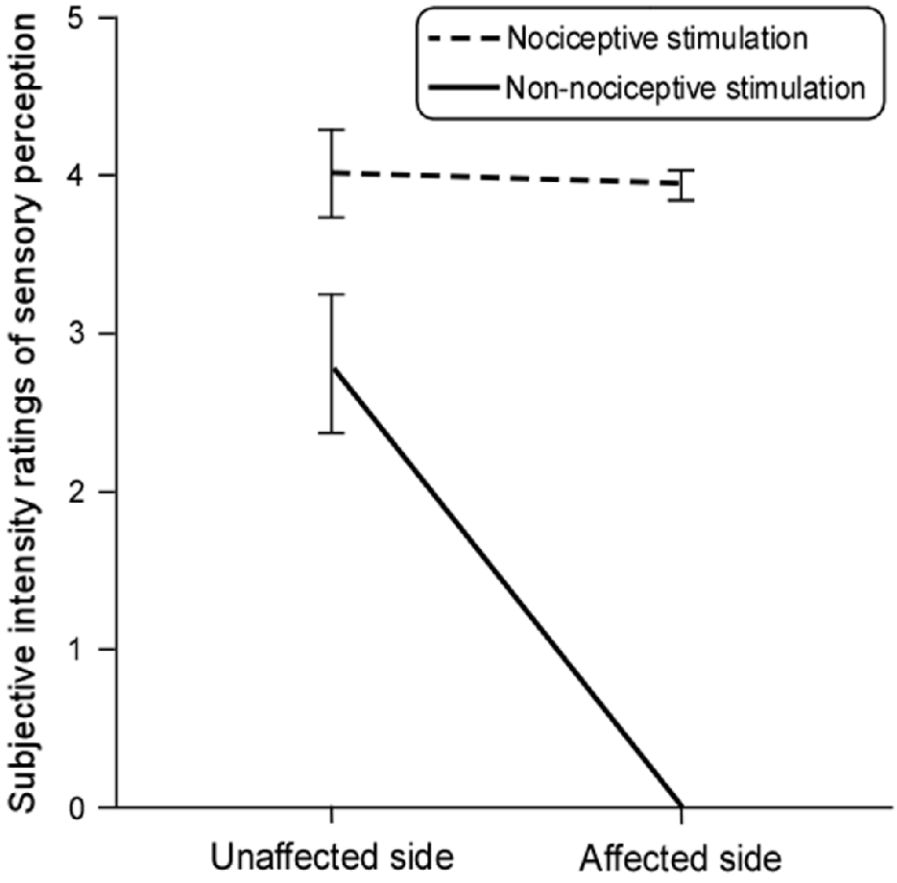

Figure 1: Subjective ratings of intensity perception to nociceptive and non-nociceptive somatosensory stimuli delivered to the unaffected and affected hands of the patient. While the nociceptive stimuli delivered to both unaffected and affected hands were equally perceived, non- nociceptive somatosensory stimuli were only detected at the unaffected side, but not at the affected side. Error bars: standard deviation.

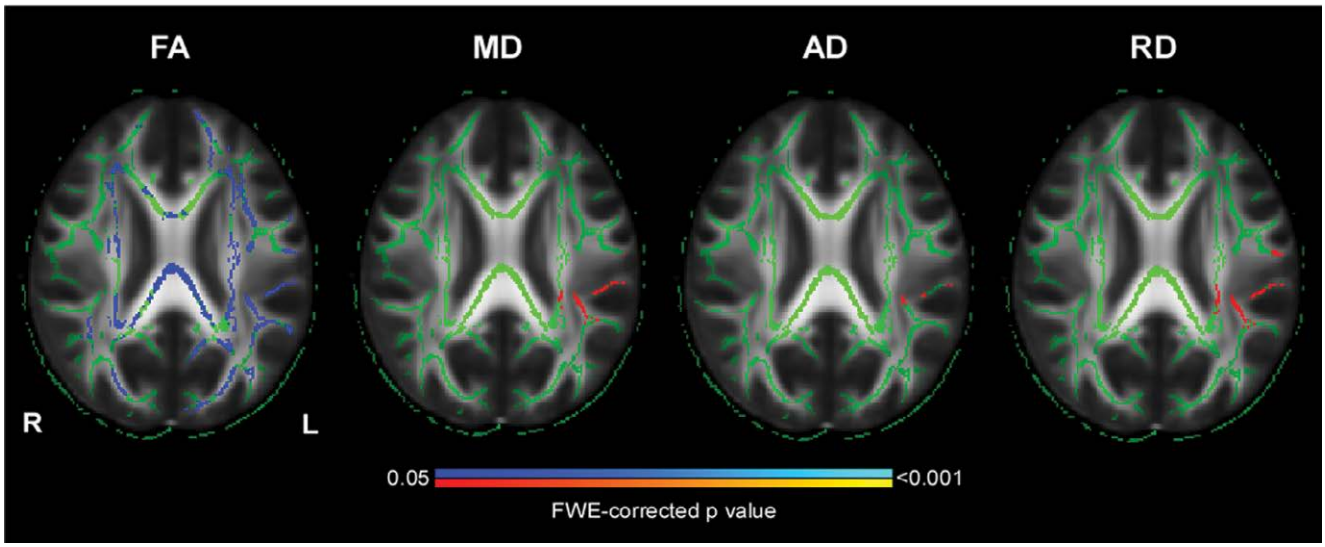

Figure 3: Tract-based spatial statistical (TBSS) analysis of fractional anisotropy (FA), mean diffusivity (MD), axial diffusivity (AD), and radial diffusivity (RD) differences between the CPSP patient and healthy subjects, controlling for age and gender. Areas in blue show regions where FA was significantly lower in the CPSP patient than healthy subjects. Areas in red show regions where MD, AD, and RD were significantly higher in the CPSP patient than healthy subjects. Clusters are significant at the level of p<0.05 after correcting for multiple comparisons using threshold-free cluster enhancement (TFCE) with a family-wise error (FWE) correction (5,000 permutations). The color bar represents the FWE-corrected p value of prediction interval test of the corresponding values, with increases in red-yellow and decreases in blue-iced blue. The axial slices depicted correspond to Z=24 in the MNI space. L: left, R: right.

Table 1: White matter clusters showing significant differences between the CPSP patient and healthy subjects in the TBSS analysis (p<0.05, FWE-corrected).

Measures	White matter clusters	Description
FA	Bilateral body of corpus callosum	Connecting the anterior and posterior portions of the corpus callosum
	Bilateral splenium of corpus callosum	Posterior structure of the corpus callosum
	Bilateral corona radiata	Includes anterior, superior, and posterior portions of the corona radiata
	Bilateral internal capsule	Includes anterior limb, posterior limb, and retrolenticular part of the internal capsule
	Bilateral external capsule	Between the thalamus and insular cortex
RD	Left posterior limb of internal capsule	Temporal WM adjacent to insular cortex
Overlapping (FA&MD&RD)	Left postcentral gyrus	Parietal WM adjacent to BA 43
	Left superior longitudinal fasciculus	Parietal WM adjacent to BA 40 and BA 2
	Left posterior corona radiata	Parieto-temporal WM adjacent to insular cortex and superior corona radiata
	Left posterior thalamic radiation	Parieto-temporal WM adjacent to insular cortex
	Left retrolenticular part of internal capsule	Temporal WM adjacent to insular cortex

TBSS: tract-based spatial statistics; FWE: family-wise error; FA: fractional anisotropy; MD: mean diffusivity; RD: radial diffusivity; WM: white matter; BA: Brodmann area.

in the CPSP patient, as compared to healthy control subjects (Table 2). The patient showed significantly lower FA values in the bilateral ACC, bilateral AI, bilateral PI, bilateral SI and SII, as well as left THA (p<0.0001, Bonferroni-corrected), compared to healthy control subjects. In addition, the patient showed significantly higher MD, AD, and RD values in the overlapped areas of left AI, left PI, left SII, bilateral ACC, and bilateral SI (p<0.0042, Bonferroni-corrected). Additional increased RD values were also observed in the left THA (p<0.0042, Bonferroni-corrected).

■ ReHo and functional connectivity analysis

Prediction interval tests on ReHo maps revealed

Table 2: Comparison of DTI measures in specific brain regions between the CPSP patient and healthy subjects.

Measures	Brain regions	Healthy controls (M ± SD)	CPSP patient	t value	*p* value
FA	Left ACC	0.23 ± 0.01	0.20	13.76	0.000**
	Right ACC	0.21 ± 0.02	0.19	9.49	0.000**
	Left AI	0.18 ± 0.01	0.16	9.24	0.000**
	Right AI	0.14 ± 0.01	0.13	4.17	0.001*
	Left PI	0.22 ± 0.01	0.18	16.06	0.000**
	Right PI	0.12 ± 0.01	0.10	9.54	0.000**
	Left SI	0.20 ± 0.01	0.14	27.29	0.000**
	Right SI	0.20 ± 0.01	0.18	11.49	0.000**
	Left SII	0.14 ± 0.01	0.11	18.01	0.000**
	Right SII	0.14 ± 0.01	0.13	6.81	0.000**
	Left thalamus	0.26 ± 0.02	0.22	8.01	0.000**
	Right thalamus	0.27 ± 0.02	0.26	1.21	0.243
MD (10^{-3} mm^2/s)	Left ACC	1.01 ± 0.11	1.13	-4.75	0.000**
	Right ACC	1.10 ± 0.13	1.22	-3.99	0.001*
	Left AI	1.37 ± 0.15	1.62	-7.47	0.000**
	Right AI	1.17 ± 0.17	1.23	-1.51	0.149
	Left PI	1.07 ± 0.11	1.67	-25.36	0.000**
	Right PI	1.30 ± 0.22	1.42	-2.57	0.019
	Left SI	0.89 ± 0.13	1.29	-13.80	0.000**
	Right SI	0.91 ± 0.09	1.02	-5.69	0.000**
	Left SII	1.08 ± 0.16	2.04	-26.42	0.000**
	Right SII	1.08 ± 0.18	1.07	0.26	0.801
	Left thalamus	1.25 ± 0.28	1.45	-3.154	0.005
	Right thalamus	1.16 ± 0.29	1.04	1.85	0.080
AD (10^{-3} mm^2/s)	Left ACC	1.25 ± 0.11	1.34	-3.64	0.002*
	Right ACC	1.33 ± 0.14	1.44	-3.55	0.002*
	Left AI	1.57 ± 0.15	1.82	-7.26	0.000**
	Right AI	1.32 ± 0.17	1.37	-1.29	0.213
	Left PI	1.28 ± 0.11	1.88	-24.20	0.000**
	Right PI	1.43 ± 0.23	1.54	-2.23	0.038
	Left SI	0.89 ± 0.13	1.29	-13.80	0.000**
	Right SI	0.91 ± 0.09	1.02	-5.69	0.000**
	Left SII	1.08 ± 0.16	2.04	-26.41	0.000**
	Right SII	1.08 ± 0.17	1.07	0.25	0.801
	Left thalamus	1.53 ± 0.29	1.70	-2.67	0.015
	Right thalamus	1.43 ± 0.29	1.29	2.18	0.042

RD (10^{-3} mm^2/s)	Left ACC	0.89 ± 0.11	1.02	-5.313	0.000**
	Right ACC	0.99 ± 0.13	1.11	-4.21	0.000**
	Left AI	1.27 ± 0.15	1.52	-7.56	0.000**
	Right AI	1.10 ± 0.16	1.16	-1.62	0.122
	Left PI	0.97 ± 0.10	1.56	-25.90	0.000**
	Right PI	1.23 ± 0.22	1.36	-2.75	0.013
	Left SI	0.80 ± 0.13	1.21	-14.65	0.000**
	Right SI	0.81 ± 0.08	0.94	-6.68	0.000**
	Left SII	1.01 ± 0.16	1.95	-26.56	0.000**
	Right SII	1.01 ± 0.17	1.01	0.05	0.964
	Left thalamus	1.11 ± 0.28	1.32	-3.41	0.003*
	Right thalamus	1.02 ± 0.28	0.91	1.68	0.110

*p<0.0042, **p<0.0001; CPSP: central post-stroke pain; FA: fractional anisotropy; MD: mean diffusivity; AD: axial diffusivity; RD: radial diffusivity; ACC: anterior cingulate cortex; AI: anterior insula; PI: posterior insula; SI: primary somatosensory cortex; SII: secondary somatosensory cortex; M ± SD: mean ± standard deviation.

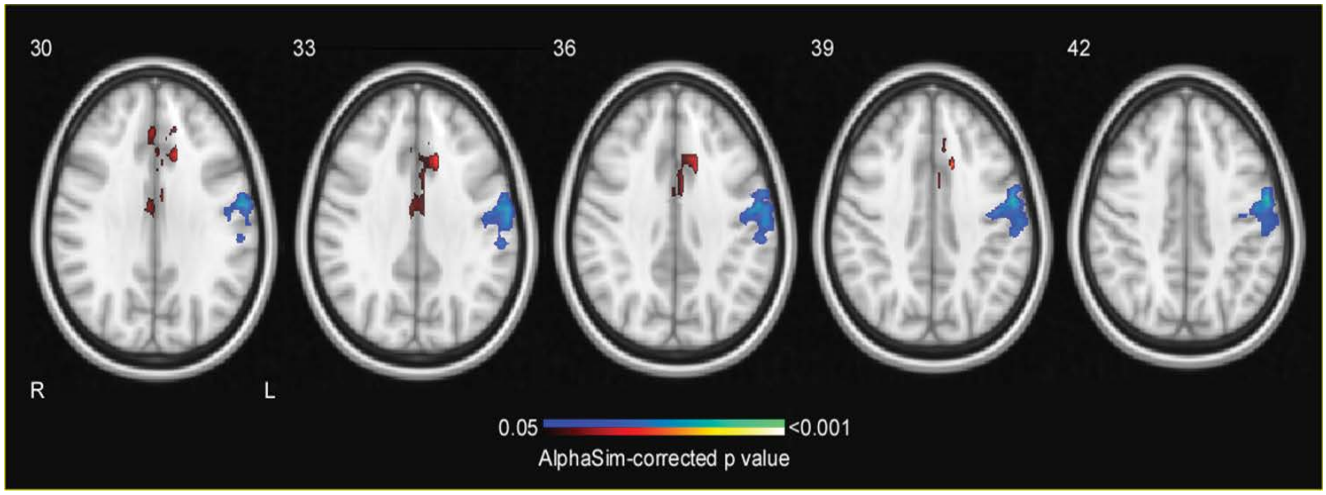

Figure 4: Differences in resting-state regional homogeneity (ReHo) values between the CPSP patient and healthy subjects, controlling for age and gender. Compared with healthy subjects, the CPSP patient showed higher ReHo in the anterior cingulate cortex (ACC), and lower ReHo in the left primary somatosensory cortex/ primary motor cortex (SI/MI) and the left secondary somatosensory cortex (SII). The threshold was set at AlphaSim-corrected p<0.05 with cluster size>202 voxels. The color bar represents the AlphaSim-corrected p value of prediction interval test of ReHo values, with increases in red-yellow and decreases in blue-iced blue. The axial slices depicted correspond to Z=30, 33, 36, 39, and 42 in the MNI space. L: left, R: right.

Table 3: Significant resting-state regional homogeneity differences between the CPSP patient and healthy subjects (p<0.05, cluster size>202 voxels, AlphaSim-corrected).

Contrast	Cluster size (voxels)	Brain regions	Peak coordinates (x, y, z)	t value
Patient > healthy subjects	227	Left ACC	-12, 12, 36	6.16
Patient < healthy subjects	420	Left SI/MI	-54, -9, 39	-5.14

ACC: anterior cingulate cortex; SI/MI: primary somatosensory cortex/ primary motor cortex; x, y, z (mm): coordinates in the MNI space.

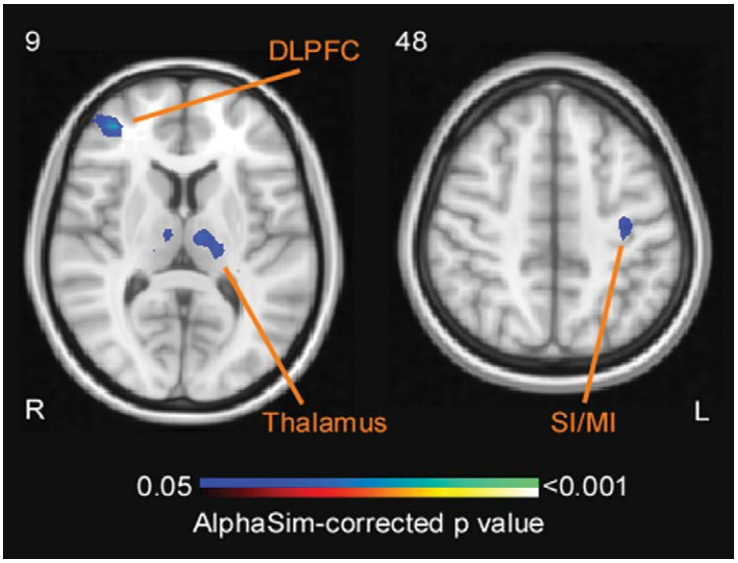

Figure 5: Differences in ACC-related functional connectivity between the CPSP patient and healthy subjects, controlling for age and gender. Compared with control subjects, the CPSP patient showed decreased functional connectivity between the ACC and the right dorsolateral prefrontal cortex (DLPFC), thalamus and left SI/MI. The threshold was set at AlphaSim-corrected p<0.05 with cluster size>202 voxels. The color bar represents the AlphaSim-corrected p value of prediction interval test of functional connectivity, with increases in red-yellow and decreases in blue-iced blue. The axial slices depicted correspond to Z=9 and 48 in the MNI space. L: left, R: right.

Table 4: Significant differences of ACC-related functional connectivity between the CPSP patient and healthy subjects (p<0.05, cluster size>202 voxels, AlphaSim-corrected).

Contrast	Cluster size (voxels)	Brain regions	Peak coordinates (x, y, z)	t value
Patient < healthy subjects	293	Right DLPFC	39, 45, 9	6.36
	424	Left superior temporal gyrus	-39, 18, -39	4.22
	332	Left thalamus	-6, -15, 6	4.10
	244	Left SI/MI	-33, -18, 48	3.29

ACC: anterior cingulate cortex; DLPFC: dorsolateral prefrontal cortex; SI/MI: primary somatosensory cortex/ primary motor cortex; x, y, z (mm): coordinates in the MNI space.

that the CPSP patient showed significantly lower ReHo values in the left somatosensory and motor cortices than healthy control subjects (left SI, left SII, and left MI; p<0.05, AlphaSim-corrected, cluster size>202 voxels; **Figure 4 and Table 3**). These reduced activating areas were in consistent with the stroke lesions of the patient. Importantly, significantly higher coherence in bilateral ACC [Brodmann area (BA) 32/24] was observed in the patient than healthy control subjects. This result suggested that functional abnormality of the ACC, the key region involving in emotional processing of pain, may be associated with the spontaneous pain of the CPSP patient.

To further explore the role of ACC in CPSP, we selected the peak voxel of ACC as the ROI for seed-based functional connectivity analysis. Prediction interval test revealed that the CPSP patient exhibited decreased functional connectivity between ACC and right dorsolateral prefrontal cortex (DLPFC), left superior temporal gyrus, left thalamus, and left SI/MI, compared with healthy control subjects (p<0.05, AlphaSim-corrected, cluster size>202 voxels; **Figure 5, Table 4**).

Discussion

This study aimed at investigating the behavioral-anatomical-functional alternations of a CPSP patient with stroke lesions in the left SII and left PI, using the somatosensory testing, DTI, and rsfMRI techniques. We observed that structural and functional alternations of some crucial brain regions (eg, somatosensory cortices, PI, and ACC) were likely contributed to the

somatosensory detection abnormalities and spontaneous pain in the CPSP patient.

From the anatomical point of view, DTI results showed a FA reduction along with MD and RD increment in the left postcentral gyrus, left retrolenticular part of internal capsule, and left posterior corona radiate in the CPSP patient, relative to healthy controls. As illustrated in **Figure 3**, these altered white matter regions corresponded to the residual ischemic cavity of left SII and left PI. It has been suggested that FA may represent the biomarker of microstructural integrity of white matter [12,13]. Previous DTI studies have provided abundant evidence pointing to the reduction of white matter integrity after stroke, indicated by the decrease in FA [14-16]. The present study with widespread decreases in FA also supported this viewpoint, revealing the white matter microstructural changes of the CPSP patient within the spino-thalamo-cortial pathway. Whereas MD may indicate the biomarker of membrane density [12,13]. AD and RD may indicate the degree of axonal damage and demyelination, respectively [17-19]. Elevations in MD and RD in our CPSP patient may be indicative of ischemic demyelination in the brain lesions, which is in consistent with pervious diffusion imaging studies showing that myelin disruptions may persist even in chronic stroke conditions [14,20].

ROI-based TBSS analysis revealed that the CPSP patient showed similar pattern of changes in the DTI properties in several pain-related regions, including left AI, left PI, left SII, bilateral SI and bilateral ACC **(Table 2)**. Previous studies found that the disturbance to the myelin sheathe after stroke occurred not only in the focal ischemic regions, but also in the area remote to the infract [14], as the white matter infracts can deteriorate and enlarge [21]. Collaboratively, our finding suggested that the changes in white matter regions, particularly the regions associated with pain-related information processing (i.e., left SII and left PI), may be attributed to demyelination, thereby causing the structural disconnection in the insult regions.

In addition to the structural disconnection, our CPSP patient, relative to healthy controls, showed increased regional functional connectivity (i.e., ReHo) in ACC and decreased ReHo in left SI/MI, extending to left SII **(Figure 4)**. The enhancement of ACC resting state activity have converged with results from pervious imaging studies associated with various chronic pain conditions [22], including CPSP [5,23,24]. Such hyperactivity may attribute to the role of ACC in affective-cognitive pain processing [22,25]. Particularly, hyperexcitability or spontaneous discharge of neurons in the pain-related brain regions may result in central sensitization that contributes to spontaneous pain in CPSP patients [6,26]. Moreover, the CPSP patient showed reduced ACC functional connectivity with left SI/MI, left thalamus, and right DLPFC **(Figure 5)**. Impaired inhibitory responses in chronic pain patients have been previously reported to be associated with reduced functional connectivity between ACC and other brain regions involving in pain inhibitory modulation, such as the DLPFC [27]. DLPFC is known to engage with descending pain inhibitory system, which is implemented via ACC targeting inhibitory neurons in DLPFC [28,29]. The reduced ACC-DLPFC coupling may explain a deficit in endogenous descending pain inhibition system in the CPSP patient. Alternatively, it should be noted that the observations of decreased regional functional connectivity in left SI/SII and reduced ACC-SI/MI coupling were in line with the brain lesions caused by stroke **(Figure 1)**. Such structural and functional impairments in the somatosensory regions were also reflected by the somatosensory testing results, with the disappearance of touch sensation on the affected hand **(Figure 2)**. A systematic review has confirmed that somatosensory cortices receive the projections of large-dimeter Aβ fibers, which convey tactile information via the dorsal horn and thalamus [30]. Therefore, decreased ACC connectivity with ipsilateral SI/MI and thalamus may indicate the lack of suppression of nociceptive information processing from non-nociceptive somatosensory inputs [31-33].

Taken together, the likely interpretation of our findings is that brain lesions, insulting to the spino-thalamo-cortical pathway, result in a disturbance of central pain-related network, thus leading to widespread maladaptive functional connectivity and spontaneous pain in the CPSP patient. In addition, these findings also point to the role of an imbalance between excitation and inhibition in the development of CPSP [24,34-36].

Conclusion

The current DTI and rsfMRI findings revealed a widespread structural and functional disconnection pattern in the CPSP patient. Such

neuroimaging results correspond to the behavioral outcomes of the patient, as the patient failed to detect the non-nociceptive somatosensory stimuli delivered to the affected hand. Merging results from behavioral, anatomical, and functional aspects, we speculated that cortical alterations (ie, widespread microstructural changes and demyelination) caused by ischemic lesions were likely to underlying functional deficits (ie, pain disinhibition and central sensitization) in CPSP, which led to a serial of clinical manifestations, such as, the loss of tactile sensation and the generation of spontaneous pain. In summary, our behavioral and neuroimaging findings may contribute to the maladaptive reorganization model of pain networks in CPSP rather than a simple process of focal disinhibition or hyperexcitability [2].

Disclosure

All authors declare no conflict of interest.

Funding

This study was funded by the National Natural Science Foundation of China (31671141).

References

1. Klit H, Finnerup NB, Jensen TS. Central post-stroke pain: clinical characteristics, pathophysiology, and management. *Lancet. Neurol* 8(9),857-868 (2009).
2. Hosomi K, Seymour B, Saitoh Y. Modulating the pain network -- neurostimulation for central poststroke pain. *Nat. Rev. Neurol* 11(5),290-299 (2015).
3. Henry JL, Lalloo C, Yashpal K. Central post-stroke pain: an abstruse outcome. *Pain. Res. Manag* 13(1),41-49 (2008).
4. Kumar G, Soni CR. Central post-stroke pain: current evidence. *J. Neurol. Sci* 284(1),10-17 (2009).
5. Peyron R, Garcia-Larrea L, Gregoire M, *et al.* Allodynia after lateral-medullary (Wallenberg) infarct. A PET study. *Brain* 121(2),345-356 (1998).
6. Vestergaard K, Nielsen J, Andersen G, *et al.* Sensory abnormalities in consecutive, unselected patients with central post-stroke pain. *Pain* 61(2),177-186 (1995).
7. Campbell JN, Meyer RA. Mechanisms of neuropathic pain. *Neuron* 52(1),77-92 (2006).
8. Craig A, Bushnell M. The thermal grill illusion: unmasking the burn of cold pain. *Science* 265(5169),252-256 (1994).
9. Wiech K, Jbabdi S, Lin C, *et al.* Differential structural and resting state connectivity between insular subdivisions and other pain-related brain regions. *Pain* 155(10),2047-2055 (2014).
10. Cauda F, D'agata F, Sacco K, *et al.* Functional connectivity of the insula in the resting brain. *NeuroImage* 55(1),8-23 (2011).
11. Song X, Dong Z, Long X, *et al.* REST: a toolkit for resting-state functional magnetic resonance imaging data processing. *PLoS. One* 6(9),e25031 (2011).
12. Beaulieu C. The basis of anisotropic water diffusion in the nervous system–a technical review. *NMR. In. Biomed* 15(7-8), 435-455 (2002).
13. Smith SM, Jenkinson M, Johansen-Berg H, *et al.* Tract-based spatial statistics: voxelwise analysis of multi-subject diffusion data. *NeuroImage* 31(4),1487-1505 (2006).
14. Borich M, MacKay A, Vavasour I, *et al.* Evaluation of white matter myelin water fraction in chronic stroke. *NeuroImage* 2,569-580 (2013).
15. Lindenberg R, Renga V, Zhu L, *et al.* Structural integrity of corticospinal motor fibers predicts motor impairment in chronic stroke. *Neurology* 74(4),280-287 (2010).
16. Stinear CM, Barber PA, Smale PR, *et al.* Functional potential in chronic stroke patients depends on corticospinal tract integrity. *Brain* 130(1),170-180 (2007).
17. Burzynska AZ, Preuschhof C, Bäckman L, *et al.* Age-related differences in white matter microstructure: region-specific patterns of diffusivity. *NeuroImage* 49(3),2104-2112 (2010).
18. Song SK, Sun SW, Ju WK, *et al.* Diffusion tensor imaging detects and differentiates axon and myelin degeneration in mouse optic nerve after retinal ischemia. *NeuroImage* 20(3),1714-1722 (2003).
19. Song SK, Sun SW, Ramsbottom MJ, *et al.* Dysmyelination revealed through MRI as increased radial (but unchanged axial) diffusion of water. *NeuroImage* 17(3),1429-1436 (2002).
20. Sotak CH. Nuclear magnetic resonance (NMR) measurement of the apparent diffusion coefficient (ADC) of tissue water and its relationship to cell volume changes in pathological states. *Neurochem. Int* 45(4),569-582 (2004).
21. Gouw AA, van der Flier WM, Pantoni L, *et al.* On the Etiology of Incident Brain Lacunes. *Stroke* 39(11),3083-3085 (2008).
22. Peyron R, Laurent B, Garcia-Larrea L. Functional imaging of brain responses to pain. A review and meta-analysis (2000). *Neurophysiol. Clin* 30(5),263-288 (2000).
23. Lorenz J, Kohlhoff H, Hansen H-C, *et al.* Aβ-fiber mediated activation of cingulate cortex as correlate of central post-stroke pain. *Neuroreport* 9(4),659-663 (1998).
24. Seghier ML, Lazeyras F, Vuilleumier P, *et al.* Functional magnetic resonance imaging and diffusion tensor imaging in a case of central poststroke pain. *J. Pain* 6(3),208-212 (2005).
25. Rainville P, Duncan GH, Price DD, *et al.* Pain affect encoded in human anterior cingulate but not somatosensory cortex. *Science* 277(5328),968-971 (1997).
26. Goto T, Saitoh Y, Hashimoto N, *et al.* Diffusion tensor fiber tracking in patients with central post-stroke pain; correlation with efficacy of repetitive transcranial magnetic stimulation. *Pain* 140(3),509-518 (2008).
27. Wiech K, Ploner M, Tracey I. Neurocognitive aspects of pain perception. *Trends. Cogn. Sci* 12(8), 306-313 (2008).
28. Lorenz J, Minoshima S, Casey K. Keeping pain out of mind: the role of the dorsolateral prefrontal cortex in pain modulation. *Brain* 126(5),1079-1091 (2003).
29. Medalla M, Barbas H. Synapses with inhibitory neurons differentiate anterior cingulate from dorsolateral prefrontal pathways associated with cognitive control. *Neuron* 61(4), 609-620 (2009).
30. Abraira VE, Ginty DD. The sensory neurons of touch. *Neuron* 79(4), 618-639 (2013).
31. Inui K, Tsuji T, Kakigi R. Temporal analysis of cortical mechanisms for pain relief by tactile stimuli in humans. *Cereb. Cortex* 16(3), 355-365 (2005).
32. Mancini F, Beaumont A-L, Hu L, *et al.* Touch inhibits subcortical and cortical nociceptive responses. *Pain* 156(10), 1936 (2015).

33. Mancini F, Nash T, Iannetti GD, *et al.* Pain relief by touch: a quantitative approach. *Pain* 155(3), 635-642 (2014).

34. Willoch F, Schindler F, Wester HJ, *et al.* Central poststroke pain and reduced opioid receptor binding within pain processing circuitries: a [11 C] diprenorphine PET study. *Pain* 108(3), 213-220 (2004).

35. Corbetta D, Sarasso, E, Agosta F, *et al.* Mirror therapy for an adult with central post-stroke pain: a case report. *Arch. Physiother* (2018).

36. Osumi M, Sumitani M, Otake Y, *et al.* A "matched" sensory reference can guide goal-directed movements of the affected hand in central post-stroke sensory ataxia. *Exp. Brain Res* (2018).